Published in final edited form as:
Neurosci Lett. 2007 February 2; 412(3): 227–232.

Major Defects in Neocortical GABAergic Inhibitory Circuits in Mice Lacking the Fragile X Mental Retardation Protein

Leah Selby[1], **Chunzhao Zhang**[1], and **Qian-Quan Sun**[1,2,*]

1 *Department of Zoology and Physiology, University of Wyoming, University of Wyoming, Laramie, WY 82071*

2 *Neuroscience Program, University of Wyoming, University of Wyoming, Laramie, WY 82071*

Abstract

This study focused on the cytoarchitectonic and morphological differences in GABA-releasing interneurons between adult Fmr1 knock-out (FMR1KO) and wild-type (WT) mice in the somatosensory cortex. Our results showed a robust reorganization of neocortical, but not hippocampal inhibitory circuits in the FMR1KO mouse. The reorganization is characterized by a significant reduction (20%, $p<0.001$) in the densities of parvalbumin (PV)-positive, but not calbindin (CB) and calretinin (CR)-positive interneurons. A significant enlargement of soma size and an altered lamina distribution of PV but not CR and CB cells was also observed. Additionally, there was a modest but significant increase in TrkB-immunoreactivity in PV-positive cells in the FMR1KO mouse. These results provide the first report showing significant alterations of GABA-releasing interneurons in the mouse model of fragile-X syndrome. Uncovering the changes in specific GABAergic inhibitory circuits could help understand mechanisms underlying the behavior deficits of fragile-X syndrome.

Keywords

GABA; inhibitory network; FMR1; somatosensory cortex

Fragile X syndrome (FXS) is the number one inherited cause of mental retardation affecting 1 in 4000 males and 1 in 8000 females (Crawford et al., 2001). Behavioral deficits of FXS include mental retardation, attention deficit, hyperactivity, anxiety, autistic behaviors and an increased incidence of epilepsy (Bear et al., 2004; Grossman et al., 2006; Frankland et al., 2004). One of the most common clinical features of FXS is heightened sensitivity to sensory stimulation (or sensory defensiveness; Miller et al., 1999; Chen and Toth, 2001; Miller, 2006). Altered sensitivity to sensory stimulation might reflect underlying abnormalities in the sensory circuits. Anatomical analyses of dendritic spine properties in adult FXS patients and FMRP KO mice have consistently demonstrated various abnormalities in the length and shape of dendritic spines of cortical excitatory neurons (Galvez et al., 2003; Irwin et al., 2000; Hinton et al., 1991). Balanced excitation and inhibition is critical for maintaining the integrity and function of neocortical circuits (Jiao et al., 2006). Deficit in GABAergic inhibitory system have been linked to epilepsy, autistic-like syndromes and sensory motor gating (Levitt, 2005). To our knowledge, there are no reports available on the effects of FMRP on the GABA-ergic interneurons. In a few recent studies, reduced expression of $GABA_A$ receptors, or enhanced

* Author of correspondence email neuron@uwyo.edu, telephone 307 766 5602, fax 307 766 5526..

epileptogensis was reported in FMR1KO mice (El Idrissi et al., 2005; Levitt, 2005; Gantois et al., 2006; Chuang et al., 2005). However, it is unclear whether GABA releasing interneurons exhibit abnormal properties in the FMR1KO mouse. This study focused on the cytoarchitectonic and morphological differences of GABA-ergic interneurons between FMR1KO and wild-type (WT) mice in the somatosensory cortex.

Materials and Methods

Mice used in this study were initially generated in Dr. William T. Greenough's lab at University of Illinois, Urbana, Illinois. To generate the mice used in the present experiment, FMR1KO mice, originally obtained from the Dutch-Belgian Fragile X Consortium [1994] were backcrossed six times with inbred C57BL/6J mice, selecting for the knockout. Eight of these adult (postnatal day 365–380; 4 WT and 4 FraX littermate) C57BL/6J (129P2-fmr1tm1Cgr) mice were transcardially perfused with 0.9% saline, pH7.4. Brains were post-fixed after perfusion in 4% paraformaldehyde at 4°C overnight, cryoprotected in 30% sucrose for 2 days, frozen, and cut into 30 μm thick cryostat sections. Free-floating sections were then stained for antibody-DAB as follows: sections were rinsed in PBS, incubated for 30 minutes in 0.5% H_2O_2 in PBS, 2 × 10 minutes PBS washes, incubated for 2 hours at room temperature in PBS with 0.3% Triton X-100, 0.05% Tween, and 4% normal goat serum, and incubated overnight at 4°C in PBS containing 0.2% Triton X-100 and primary antibodies directed against: PV (1:1000, Calbiochem, San Diego, CA). Sections were then rinsed two times in PBS, incubated at room temperature for 90 minutes in PBS containing biotinylated goat anti-rabbit IgG (Vector labs) for PV, and finally incubated overnight at 4°C in Vectastain ABC kit (Vector Labs). Sections were then rinsed two times in PBS, developed in 50mM TBS containing 0.04% 3,3′-diaminobenzidine tetrahydrochloride (DAB, Sigma, St. Louis, MO) and 0.012% H_2O_2 washed two times with TBS, mounted onto glass slides, dehydrated, cleared and coversliped. For double-immunohistochemical staining, sections were rinsed in PBS, incubated for 30 minutes in 0.5% H_2O_2 in PBS, washed 2 × 10 minutes in PBS, incubated for 2 hours at room temperature in PBS with 0.3% Triton X-100, 0.05% Tween, and 4% Normal Goat Serum, and incubated overnight at 4°C in PBS containing 0.2% Triton X-100 and primary antibodies directed against PV (1:1000, Calbiochem, San Diego, CA). The other primary antibodies used were: a polyclonal rabbit anti-TrKB (1:250, Santa Cruz Biotechnology), a polyclonal rabbit anti-calretinin antibody (1:500, Sigma), a polyclonal rabbit anti-calbindin antibody (1:1000, Sigma). Sections were then rinsed two times in PBS, incubated for 3 hours at room temperature in Alexa Fluor 594, goat anti-rabbit IgG (H+L) for PV. The sections were then rinsed, mounted and coversliped using Vectashield mounting medium with DAPI or without DAPI. The immunofluorescent specimens were examined using an epifluorescence microscope (Carl Zeiss) equipped with AxioCam digital color camera. Double or triple immunofluorescent images were analyzed using an AxioVision LE imaging suite (Carl Zeiss). Confocal microscopy images were sampled using an upright Nikon E800 microscope and Bio-Rad Radiance 2100 image analysis software suits. Cell counting and cell area measurements were performed with Automeasure® function (part of AxioVision LE imaging suite, Carl Zeiss). Morphometric measurement parameters are generated by the contour of the DAB stained cells. The software uses the binary image as a mask to calculate geometric and densitometric parameters from the original image. Their export into Excel enables statistical information about specimen details. An example of the cell counting function of this program was shown in Fig 4A3, where each cell identified by the Automeasure® program was demarcated with red colored lines. We regularly verified the cell count to ensure its accuracy. The area of the cells was also provided by the Automeasure® program and was exported into Excel® where statistical information about specimen details were analyzed. We validated the areas detected by the Automeasure® program with areas measured by the Neurolucida function (MicroBrightField, e.g. Fig 1B2). The results obtained from the two different methods overlapped very well. The measurement of TrKB immunoreactivity was also performed via

the same Automeasure® program. More specifically, the cells were first identified and outlined (e.g. Fig 4A3). The gray scale fluorescent intensity for TrKB-IR (red) was then measured and exported to Excel®. This measure has been used successfully in experience-dependent plasticity of GAD-IR in barrel cortex (Jiao et al., 2006).

Results and Discussions

We first made sure the two TC sections from the WT and FMR1KO mice matched with each other. This was achieved via a quantitative analysis method using Neurolucida®. Typically, outlines of the TC sections of WT and FMR1KO mice were traced separately and aligned to ensure the two sections matched. As shown in Fig 1A2 and its inset, the area of the two sections we analyzed was essentially the same. PV-expressing interneurons in the somatosensory cortex were compared between the wild-type and FMR1-KO mice. Four control brains and four FMR1-KO brains were studied (Fig. 1). Slices were processed for DAB staining and cells stained positive for PV antibodies were analyzed. In all sections (2 sections per brain), FMR1KO mice (205± 20 cells/mm^2) showed a down-regulation of PV positive neurons compared to the WT mice (251± 16cells/mm^2). The down-regulation of PV cell in FMR1KO mice was statistically very significant ($P<0.0001$, n=8 sections from 4 brains, Fig 2A2 vs. A1 and C2; Fig 3A2 vs. A1 & Fig 4B1 vs. A1). Size of PV neurons was determined by measuring cell area using Automeasure® function of the AxioVision LE imaging suite (Carl Zeiss). As shown in Fig. 2 (B1 vs. B2 and C1), the average soma area of PV neurons in FMR1KO mice was larger than that of WT mice and the difference was statistically significant ($P<0.001$, n=8 sections from 4 brains). Distribution of soma size of PV neurons in WT vs. FMK1KO mice was shown in Fig 2C1. Distribution of PV neurons in layers II/III, IV, V, and VI were shown in Fig. 3. Double immunohistochemistry and DAPI staining were used on sections of the somatosensory cortex. DAPI positive cells were used to determine the cortical lamination. PV-positive cells were counted in each layer and the distribution was compared (2 brains for FMR1KO and WT, 4 sections each). The FMR1KO mice showed a decrease of PV neurons in Layer II/III (6.9±1.2% vs. 11.6±2.1%, $p<0.001$), a decrease in Layer IV (6.4±1.1% vs. 16.1 ±1.5%, $p<0.001$), an increase in Layer V (61.4±3.4% vs. 52±4.2%, $p<0.05$) and an increase in Layer VI (25.3±2.4% vs. 20.3±2.6%, $p<0.05$, Fig. 3A1 vs. A2). We conclude that FMR1KO mice showed a marked increase in distribution of PV-expressing neurons toward deeper layers (V and VI, Fig. 3A1 vs. A2, C1). In contrast, CB- and CR-positive neurons showed no difference in layer counts between the FMR1KO mouse and the WT mouse (Fig. 3C2).

The numerical and area measurements of calbindin-expressing and calretinin-expressing neurons were measured using the same techniques. One brain for both the FMR1KO and WT mice were sliced and cells were counted on two sections. In the FMR1KO mouse the CB-cell count (15±4 cells/mm^2, n=4 sections) was not significantly different from the CB count in the WT mouse (12±6 cells/mm^2, n=4 sections). For CR-cell count the FMR1KO mouse (76±8cells/mm^2, n=4 sections) was not significantly different from the WT mouse (91±12 cells/mm^2, n=4 sections). There was no statistically significant difference ($P=0.8629$) in the areas of CR neurons in FMR1KO mice (103 ± 39 μm^2) and WT mice (105 ± 36 μm^2). CB-positive neurons had no statistically significant difference in area between FMR1KO mice (116 ± 37 μm^2) and WT mice (136 ± 44 μm^2 see Fig. 2C3). The results with diameter of PV, CB and CR cells are consistent with the area measurements in these cells, except that the diameter for CB cells is significantly smaller (Fig 3C4). In summary, we conclude that in the FMR1KO mouse, the number of PV-positive interneurons was significantly reduced in numbers but greater in size than the WT mice. The count and area of the CB- and CR-positive neurons did not differ significantly between the FMR1KO mouse and the WT mouse.

The numerical and area measurements of PV-expressing neurons in the dentate gyrus and the CA1 areas of the hippocampus were also measured. Two brains for both the FMR1KO and

WT mice were sliced and cells counted on three sections. The PV cell count in the FMR1KO mouse (14.65 ± 5.29 cells/mm^2, n=6 sections from two brains) was not significantly different from the PV count in the WT mouse (14.59 ± 2.16 cells/mm^2, n= 6 sections from two brains). In the CA1 region, PV count in the FMR1KO mouse (20.18 ± 5.29 cells/mm^2) was not significantly different (P>0.5) from the PV count in the WT mouse (21.89 ± 7.99 cells/mm^2, n= 6 sections from two brains). In the dentate gyrus, there was no statistical difference (P >0.5) in the areas of PV neurons in the FMR1KO mice (264 ± 109 μm^2, n= 6 sections from two brains) and WT mice (343 ± 175 μm^2, n= 6 sections from two brains). In the CA1, there was no statistical difference (P >0.5) in the areas of PV neurons in the FMR1KO mice (198 ± 104 μm^2 n= 6 sections from two brains) and WT mice (203 ± 62 μm^2 n= 6 sections from two brains). The count and area of the PV-positive neurons did not differ significantly (p>0.5) between the FMR1KO and WT mice.

FMR1 proteins are known to interact with neurotropic factors such as BDNF and regulate the plasticity of neural development (Castren et al., 2002). To test whether receptors for BDNF show altered expression in FMR1KO mouse, especially in GABA releasing interneurons, we performed double-immunohistochemical analysis. In sections from WT, tyrosine kinase receptor B (TrkB)-IRs were found predominantly in dendritic-like structures that projects perpendicularly toward the pia surface (Fig 4A2). This indicates that there is a robust expression of TrkB-IR in presumed apical dendrites of pyramidal neurons. In the FMR1KO mice, the pattern of TrkB-IR is different from controls (e.g. Fig 4B2 vs. B1). There is an apparent reduction in the number of TrkB-positive puncta oriented perpendicularly to the pia surface and a reduction in the total number of TrkB-positive puncta, as well. This is consistent with abnormal development of dendritic spines reported in FMR1KO mice (Galvez et al., 2003b; Irwin et al., 2000; Hinton et al., 1991). Next, TrkB expression in the cell bodies of PV-expressing interneurons was measured using relative intensities of TrkB staining (see Fig. 4A3). In the FMR1-KO mice, TrkB expression showed a significant up-regulation, compared to the WT-mice (p<0.001; Fig 4C). We examined this result with confocal microscopic images, as shown in insets of Fig 4A2 & B2, there are many cells in WT brain in which TrkB-IR were lower or had none.

The current study shows a robust reorganization of GABAergic circuits in the somatosensory cortex of the FMR1KO mouse. The reorganization occurs preferentially to a specific group of interneurons: PV-positive and fast-spiking interneurons. This is the first report showing specific alterations in GABA-releasing interneurons in a rodent model of fragile-X syndrome. Previously, observations of neuronal morphological abnormalities have been limited to glutamatergic neurons and their dendrites (Galvez et al., 2003; Irwin et al., 2000; Hinton et al., 1991). The changes in the inhibitory circuits in the FMR1KO are consistent with the heightened sensitivity of sensory-motor gating (Bear et al., 2004; Grossman et al., 2006; Frankland et al., 2004; Miller et al., 1999; Chen and Toth, 2001) and increased incidence of epilepsy seen in fragile-X mouse and patients (El Idrissi et al., 2005; Levitt, 2005; Gantois et al., 2006; Chuang et al., 2005). Although we have shown changes in TrKB receptor expression in PV interneurons, the exact mechanisms underlying the reorganization of PV-circuits require thorough investigations in future studies. Another notable finding about the present study was that the age of animal group. The mice we studied had an average age of 1 year old, which is equivalent to an aging human. Changes in the lamination of PV cells, particularly the deeper layers may underlie alteration of sensory-motor gating.

Acknowledgements

Leah Selby is a recipient of NSF-Wyoming--EPSCoR summer and fall undergraduate research fellowship award. This research was made possible by NIH-NCRR grant P20 RR16474-04. Confocal microscopy was performed in the University of Wyoming's Microscopy Core Facility. We thank Dr. William T. Greenough at the University of Illinois, Urbana, for generously providing the first generation of FMR-1 KO mice and their background WT strain and for providing genotyping and protocols.

References

1. Bear MF, Huber KM, Warren ST. The mGluR theory of fragile X mental retardation. Trends Neurosci 2004;27:370–377. [PubMed: 15219735]
2. Castren M, Lampinen KE, Miettinen R, Koponen E, Sipola I, Bakker CE, Oostra BA, Castren E. BDNF regulates the expression of fragile X mental retardation protein mRNA in the hippocampus. Neurobiol Dis 2002;11:221–229. [PubMed: 12460560]
3. Chen L, Toth M. Fragile X mice develop sensory hyperreactivity to auditory stimuli. Neuroscience 2001;103:1043–1050. [PubMed: 11301211]
4. Chuang SC, Zhao W, Bauchwitz R, Yan Q, Bianchi R, Wong RK. Prolonged epileptiform discharges induced by altered group I metabotropic glutamate receptor-mediated synaptic responses in hippocampal slices of a fragile X mouse model. J Neurosci 2005b;25:8048–8055. [PubMed: 16135762]
5. El Idrissi A, Ding XH, Scalia J, Trenkner E, Brown WT, Dobkin C. Decreased GABA(A) receptor expression in the seizure-prone fragile X mouse. Neurosci Lett 2005;377:141–146. [PubMed: 15755515]
6. Frankland PW, Wang Y, Rosner B, Shimizu T, Balleine BW, Dykens EM, Ornitz EM, Silva AJ. Sensorimotor gating abnormalities in young males with fragile X syndrome and Fmr1-knockout mice. Mol Psychiatry 2004;9:417–425. [PubMed: 14981523]
7. Galvez R, Gopal AR, Greenough WT. Somatosensory cortical barrel dendritic abnormalities in a mouse model of the fragile X mental retardation syndrome. Brain Res 2003;971:83–89. [PubMed: 12691840]
8. Gantois I, Vandesompele J, Speleman F, Reyniers E, D'Hooge R, Severijnen LA, Willemsen R, Tassone F, Kooy RF. Expression profiling suggests underexpression of the GABA(A) receptor subunit delta in the fragile X knockout mouse model. Neurobiol Dis 2006a;21:346–357. [PubMed: 16199166]
9. Grossman AW, Aldridge GM, Weiler IJ, Greenough WT. Local protein synthesis and spine morphogenesis: Fragile X syndrome and beyond. J Neurosci 2006;26:7151–7155. [PubMed: 16822971]
10. Hinton VJ, Brown WT, Wisniewski K, Rudelli RD. Analysis of neocortex in three males with the fragile X syndrome. Am J Med Genet 1991b;41:289–294. [PubMed: 1724112]
11. Irintchev A, Rollenhagen A, Troncoso E, Kiss JZ, Schachner M. Structural and functional aberrations in the cerebral cortex of tenascin-C deficient mice. Cereb Cortex 2005;15:950–62. [PubMed: 15537675]
12. Irwin SA, Galvez R, Greenough WT. Dendritic spine structural anomalies in fragile-X mental retardation syndrome. Cereb Cortex 2000c;10:1038–1044. [PubMed: 11007554]
13. Jiao Y, Zhang C, Yanagawa Y, Sun QQ. Major effects of sensory experiences on the neocortical inhibitory circuits. J Neurosci 2006;26:8691–701. [PubMed: 16928857]
14. Levitt P. Disruption of interneuron development. Epilepsia 46 Suppl 2005;7:22–28.
15. Miller LJ, McIntosh DN, McGrath J, Shyu V, Lampe M, Taylor AK, Tassone F, Neitzel K, Stackhouse T, Hagerman RJ. Electrodermal responses to sensory stimuli in individuals with fragile X syndrome: a preliminary report. Am J Med Genet 1999a;83:268–279. [PubMed: 10208160]
16. Ren JQ, Aika Y, Heizmann CW, Kosaka T. Quantitative analysis of neurons and glial cells in the rat somatosensory cortex, with special reference to GABAergic neurons and parvalbumin-containing neurons. Exp Brain Res 1992;92(1):1–14. [PubMed: 1486945]

Abbreviations

PV
: Parvalbumin

CB
: Calbindin

CR
: Calretinin

TrkB
: Tyrosine kinase B

WT
: Wild-type (control)

FMR1KO
: FMR1 knock-out

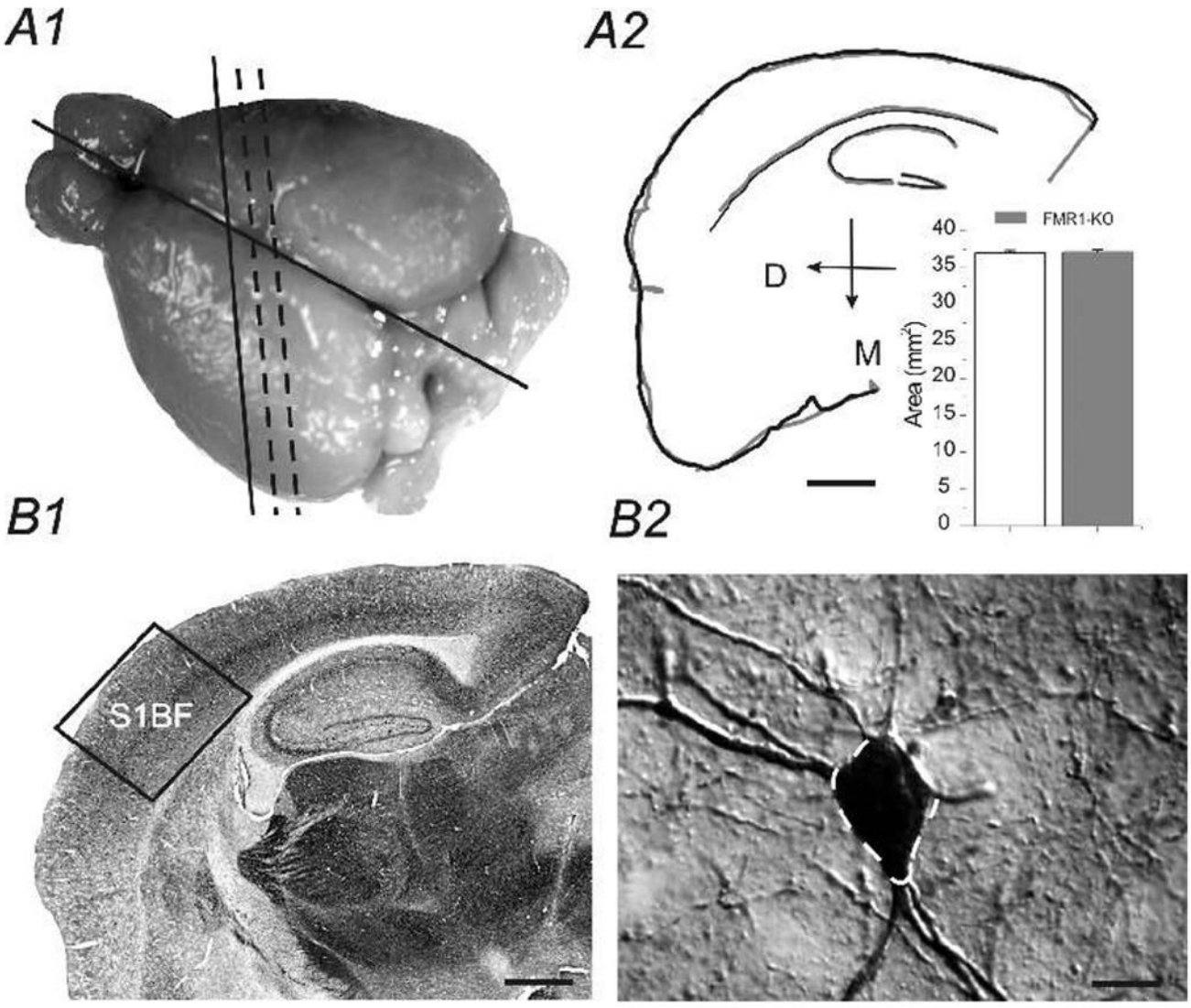

Fig. 1.

A1) Dorsal aspect of mouse brain, slightly tilted for optimal view of somatosensory cortex. black solid and dashed lines shows tilted (thalamocortical) section level for Figures 2–4. **A2)** Neurolucida traced outlines (Black: WT; Gray: FMR1KO) of the two TC sections used in a paired-analysis. Inset: areas of TC sections from WT and FMR1KO mice are essentially the same (n=2 brains in WT and FMR1KO, respectively). Scale bar=500 μm. **B1)** Virtual slice image of the entire TC section. Boxed region shows area of somatosensory barrel cortex studied (S1BF). **B2)** High resolution photomicrograph image of a parvalbumin-positive cell in the S1BF of WT mouse. Dashed outline (white) demarcate cell body area outlined by the Neurolucida tracing program. Scale bar = 5 μm.

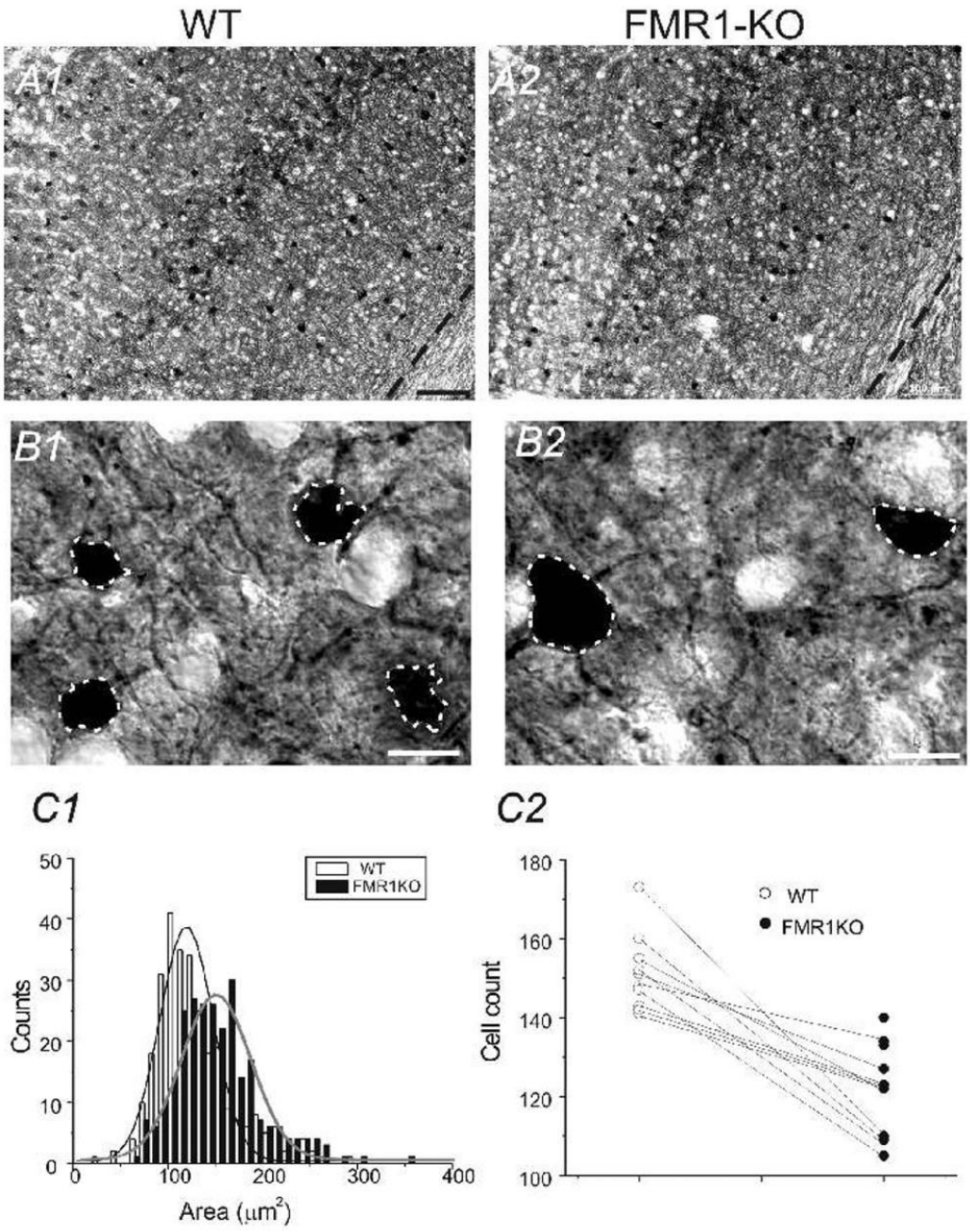

Fig. 2.

A) TC section through somatosensory cortex stained with PV antibodies. Scale bar = 100 μm. **A1)** WT brain **A2)** FMR1-KO brain; **B)** High resolution micrograph image of PV positive neurons and processes. **B1)** WT brain **B2)** FMR1-KO brain. Scale bars = 6 μm. **C1)** Histogram of distribution of PV cell areas in 4 WT mice vs. 4 FMR1-KO mice. **C2)** The number of PV-positive cells in 10 different TC sections (0.6 mm^2 per section) from 4 WT and 4 littermate FMR1KO mice.

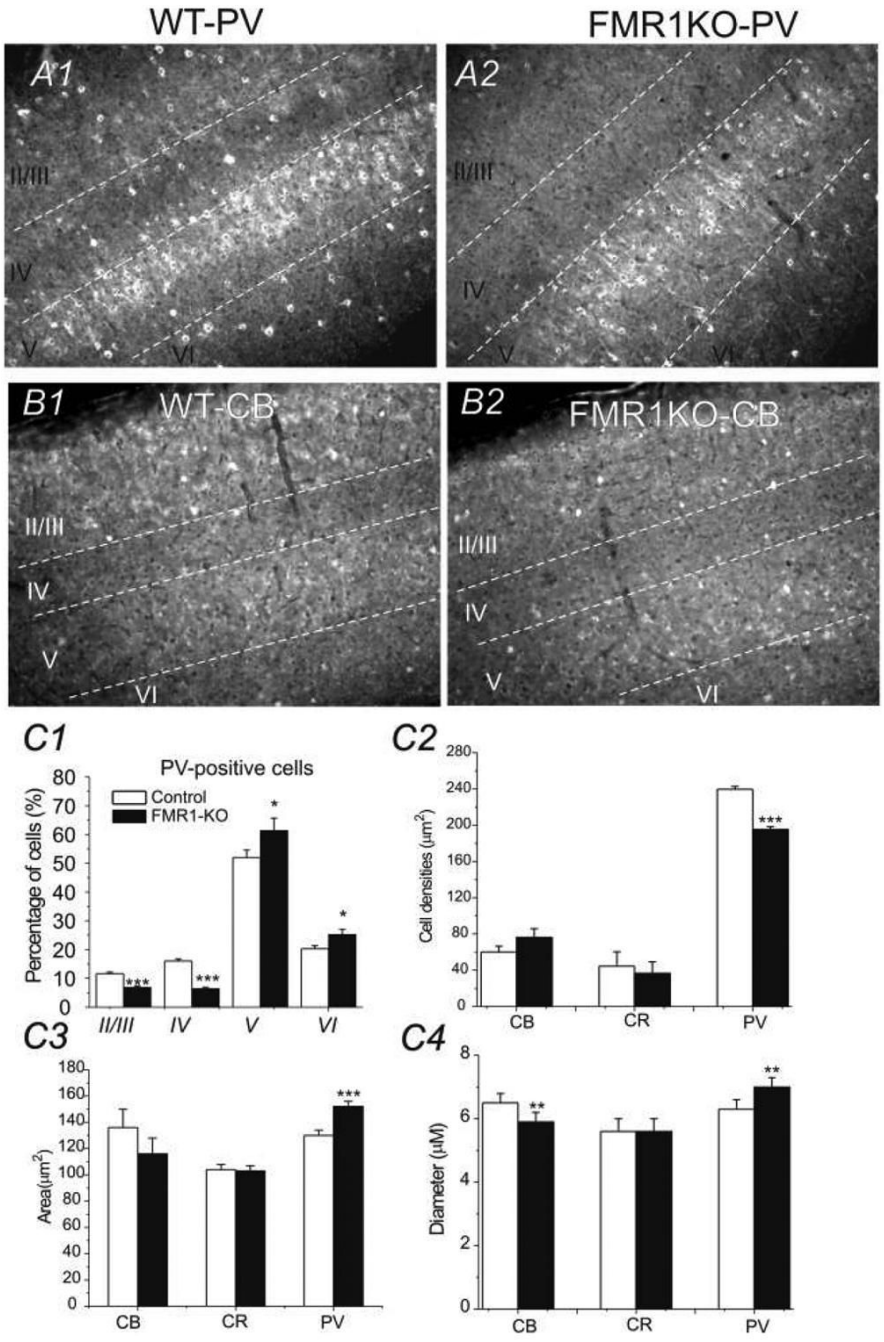

Fig. 3.

A) Photomicrograph of PV-IR in the somatosensory cortex with distinguished layers, identified via DAPI staining (not shown). Asterisks denote PV positive neurons. Scale bars =100 μm. **A1)** WT brain **A2)** FMR1-KO brain. **B)** Photomicrograph of somatosensory cortex with staining of CB antibodies. **B1)** WT brain **B2)** FMR1-KO brain; Scale bars =100 μm. **C)** Comparison of the percentage distribution of total PV-positive neurons (C1), cell densities (C2), areas (C3), and diameter (C4) in somatosensory cortex for 4 WT (white bars) and 4 FMR1-KO (black bars) brains. **: $p<0.01$; ***: $p<0.001$.

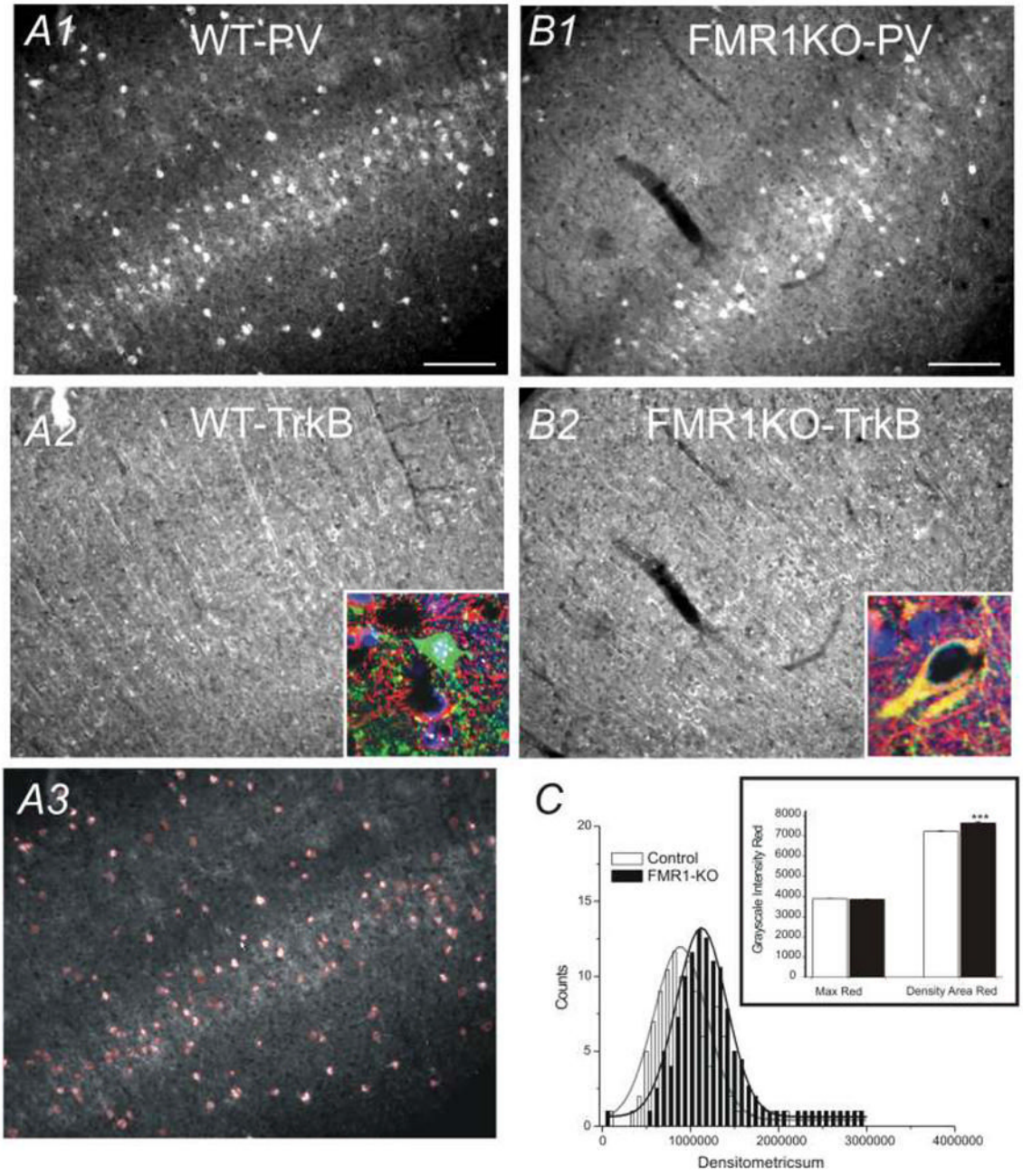

Fig. 4.

A) Photomicrograph of somatosensory cortex in WT brain. **A1)** PV-IR, **A2)** TrkB –IR, **A3)** Area of PV cell bodies demarcated by the Automeasure® program. Scale bars = 100 μm. **B)** Photomicrograph of somatosensory cortex in FMR1-KO brain. **B1)** PV staining; **B2)** TrkB staining. Insets in A2 & B2: confocal imaging of staining (green: PV-IR; red: TrkB-IR; Blue: DAPI). **C)** Histogram distribution of gray scale densities of red color intensities (TrKB-IR) per PV neuron cell in 3 WT (open bars) and 3 FMR1-KO (black bars) brains. Inset: gray scale distribution of maximum red color intensities and mean densities of red area in WT (open bars) and FMR1-KO (black bars) brains. ***:$p<0.01$, n=6 brains.